Mixed Matrix Composite Membranes with MOF-protruding Structure for Efficient CO2 Separation

Shuqing Song[1], Mingang Zhao[1], Zheyuan Guo[1], Yanxiong Ren[1], Jianyu Wang[1], Xu Liang[1], Yunchuan Pu[1], Shaoyu Wang[1], Hanze Ma[1], Xuerui Wang[2], Guangwei He[1], and Zhongyi Jiang[1]

[1]Tianjin University
[2]Nanjing Tech University

September 30, 2022

Abstract

Mixed matrix composite membranes (MMCMs) hold great potential to realize efficient CO2 removal from natural gas. However, the reduction of separation performance arising from the interfacial defects, significant plasticization and aging effect in the thin films severely limit their application. Herein, we fabricated a series of polyimide MMCMs with MOF-protruding structure wherein amino-functionalized ZIF-8 nanocrystals nearly penetrate the thin selective layer. Through engineering the interfacial interactions, e.g., covalent or hydrogen bondings, we successfully fabricated defect-free MMCMs with the thickness ranging from 140 to 280 nm. The stronger interfacial interactions eliminate the interfacial defects and restrict the mobility of polymer chains under high pressure. Accordingly, the MMCM displays a high CO2 permeance of 778 GPU and a CO2/CH4 selectivity of 34 with significantly improved resistance to plasticization and aging. Considering the superior performance, we anticipate our work could provide guidelines on designing advanced MMMs to tackle critical separations.

Mixed Matrix Composite Membranes with MOF-protruding Structure for Efficient CO_2 Separation

Shuqing Song[a,b], Mingang Zhao[a,b], Zheyuan Guo[a,b], Yanxiong Ren[a,d],Jianyu Wang[a,b], Xu Liang[a,b], Yunchuan Pu[a,d], Shaoyu Wang[a,b], Hanze Ma[a,b], Xuerui Wang[e], Guangwei He[a,b,c,*], and Zhongyi Jiang[a,b,c,d*]

[a] Key Laboratory for Green Chemical Technology of Ministry of Education, School of Chemical Engineering and Technology, Tianjin University, Tianjin 300072 (China).

[b] Collaborative Innovation Center of Chemical Science and Engineering (Tianjin), Tianjin 300072 (China).

[c] Haihe Laboratory of Sustainable Chemical Transformations (Tianjin), Tianjin 300192 (China)

[d] Joint School of National University of Singapore and Tianjin University, International Campus of Tianjin University, Binhai New City, Fuzhou 350207 (China).

[e] State Key Laboratory of Materials-Oriented Chemical Engineering, College of Chemical Engineering, Jiangsu National Synergetic Innovation Center for Advanced Materials, Nanjing Tech University, Nanjing 211816 (China).

*Corresponding authors: School of Chemical Engineering and Technology, Tianjin University, Tianjin 300072 (China).

E-mail address: *guangwei@tju.edu.cn* (Guangwei He)

E-mail address: *zhyjiang@tju.edu.cn* (Zhongyi Jiang)

Abstract

Mixed matrix composite membranes (MMCMs) hold great potential to realize efficient CO_2 removal from natural gas. However, the reduction of separation performance arising from the interfacial defects, significant plasticization and aging effect in the thin films severely limit their application. Herein, we fabricated a series of polyimide MMCMs with MOF-protruding structure wherein amino-functionalized ZIF-8 nanocrystals nearly penetrate the thin selective layer. Through engineering the interfacial interactions, e.g., covalent or hydrogen bondings, we successfully fabricated defect-free MMCMs with the thickness ranging from 140 to 280 nm. The stronger interfacial interactions eliminate the interfacial defects and restrict the mobility of polymer chains under high pressure. Accordingly, the MMCM displays a high CO_2permeance of 778 GPU and a CO_2/CH_4selectivity of 34 with significantly improved resistance to plasticization and aging. Considering the superior performance, we anticipate our work could provide guidelines on designing advanced MMMs to tackle critical separations.

Keywords: Natural gas purifications, mixed matrix membranes, thin-film composite membranes, interfacial interactions.

Introduction

Efficient CO_2 removal from natural gas has been regarded as one of the most important processes in modern chemical industries because the presence of CO_2 can reduce the calorific value and make the natural gas streams acidic and corrosive.[1-3] Among CO_2 separation processes, membrane technologies hold great potential to siginificantly increase the energy efficiencies and reduce the environmental impacts compared with traditional separation technologies such as adsorption and absorption.[3-8] To date, polymeric membranes is dominating the membrane separation market because of the ease of processing polymers into thin selective membranes.[2,9-11] Nevertheless, the separation performance of polymeric membranes suffers from the trade-off effect, as depicted by the Robeson plot for typical gas pairs including CO_2/CH_4.[12-14] In this context, it is essential to develop membranes that can outperform conventional polymeric membranes.

Metal-organic framework (MOF) based mixed matrix membrane (MMM), which combines the advantages of molecular-sieving capability of microporous fillers and solution processibility of polymers, has been widely researched as an effective approach to surpass the performance upper-bound of polymeric membranes.[14-21]Recently, MMMs with MOFs penetrating matrix have attracted extensive attention because the fillers are expected to dominate the membrane separation performance which approaches to that from pure MOF crystals.[22-25]For example, Huang and co-workers fabricated highly H_2permeable MMMs with ZIF-7 microplates penetrating the polymer matrix and yielded a 14-fold higher H_2 permeance and 9-fold higher H_2/CO_2 selectivity, respectively.[22] Our group has proposed a MMM with ZIF-8 microcrystals nearly penetrate the polyimide matrix and form a "Direct-through Channel" structure which achieves nearly 70% of C_3H_6/C_3H_8separation performance from pure ZIF-8 crystals according to the calculation results of the Maxwell model.[24] Overall, MMMs with MOF-penetrated structure are still in its infancy stage and usually a self-standing membrane with large thickness is fabricated in most studies. For practical application, mixed matrix composite membranes (MMCMs) with thin selective layers are much more attractive attributing to the fact that the thin selective layer is expected to minimize the trans-membrane resistance and thus maximize the gas permeance.[26-28] Till now, fabricating ultrathin selective films with nano-sized MOF penetrated the selective layer has been rarely reported. Wang's group developed MMMs with penetrated oligomer-grafted MIL-101 nanoparticles serving as gas transport channels in rubbery poly-vinylamine (PVAm) matrix, with a CO_2permeance of 823 GPU and a CO_2/N_2selectivity of 242 under humidified conditions.[23]

Glassy polymeric membranes have excellent mechanical/chemical stabilities which benefit the operation under extreme conditions such as high pressure.[10,11,29-32] However, the fabrication of high-performance MMCMs using glassy polymer as matrix remains elusive. In theory, there are two critical issues remaining unresolved. Firstly, non-selective defects or pinholes can be easily generated at the interfaces when the membrane thickness reduces to sub-micrometer or nanometer scale due to the weak interfacial interactions between the fillers

and rigid chains of glassy polymers which are detrimental to the separation performance.[26,27] Secondly, the plasticization and aging effect would become more serious for thin-selective layer, owing to the enhanced chain mobility of polymers, leading to drastic decrease of the overall separation performance.[29,33,34]

To overcome the above-mentioned issues, we develop a series of MMCMs, containing MOF-protruding structure wherein the MOF crystals nearly penetrate the thin selective layer. The thickness of the selective layer can be reduced to 140-280 nm through engineering the interfacial hydrogen or covalent bonds, as illustrated in Fig. 1. Attributing to the affinity of amine groups to CO_2 and low permeation resistance of the selective layer with protruding MOFs, the MMCM yields a CO_2 permeance of 778 GPU which is three-fold higher than that of polyimide membrane with a CO_2/CH_4 selectivity of 34, and demonstrated improved resistance to plasticization (up to 40 bar) and aging performance (for 28 days). Considering the superior CO_2 separation performance as well as the good resistance to plasiticization and aging, we anticipate that the MMCMs hold great potential for real applications in natural gas purification processes.

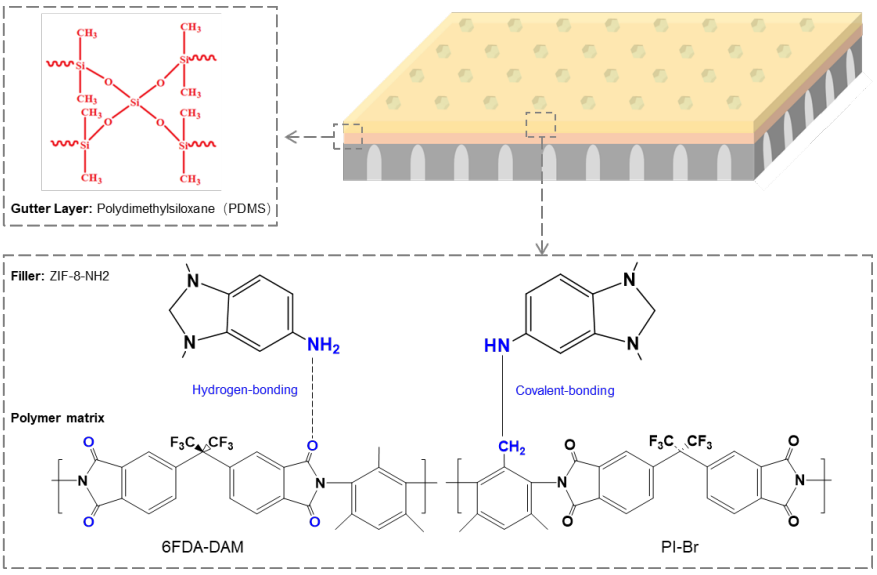

Fig. 1 Schematic diagram of this work

Experimental section

Materials

2-aminobenzimidazole ($C_7H_7N_3$, 99%, Heowns) and 2-methylimidazole ($C_4H_6N_2$, 98%, Heowns) were employed as organic linker sources of NH2-ZIF-8 nanocrystals. Zinc nitrate hexahydrate ($Zn(NO_3)_2{\cdot}6H_2O$, 97%, Meryer) was employed as the zinc source. Sodium formate (CHO_2Na, 98%, TCl) was employed for the deprotonation of imidazoles. Ethanol (C_2H_5OH, 99.5%, Jiangtian Chemical Technology), n-heptane (GC, Aladdin), dimethylacetamide ($CH_3CON(CH_3)_2$, 99.5%, Meryer, hereafter DMAc), tetrahydrofuran (C_4H_8O, GC, Meryer, hereafter THF), N, N-Dimethylformamide (C_3H_7NO, 99%, Aladdin, hereafter DMF) and deionized (DI) water were employed as solvents. Polydimethylsiloxane (PDMS, part A and B, SILGARD^{TM}184) was employed for surface modification of porous substrates. N-bromosuccinimide (NBS, 99%, Aladdin) and azodiisobutyronitrile (AIBN, 99%, Aladdin) were utilized as bromo-functionalized reagents. Triethylamine ($(C_2H_5)_3N$, 99.5%, TCl) and acetic anhydride ($C_4H_6O_3$, 99.5%, TCl) were employed as the catalyst and dehydrating reagent in the synthesis process of polyimide, respectively. Polyacrylonitrile (here-after PAN, mean pore diameter of ˜20 nm) was used as the porous substrates. All the above reagents and materials were used without further purification. Before polymerization, the monomers 6FDA ($C_{19}H_6F_6O_6$, 99.5%, Sigma-Aldrich) DAM ($C_9H_{14}N_2$, 99.5%, Sigma-Aldrich) were purified by vacuum sublimation at 215°C and

75°C, respectively.

Preparation of PDMS modified substrates (mPANs)

Firstly, we prepared 0.3 wt% PDMS solution: 0.5 g PDMS part A and 0.05 g part B were added to 109.45 g n-heptane, and the solution was stirred for 4 h. Secondly, the PAN substrates were fixed on the surface of the glass sheet by Kapton tapes, and we spread the PDMS solution to cover the surface of the substrates and started spin-coating at the spinning speed of 500, 1000, 2000 and 3000 rpm for 1min, respectively. After spin-coating process, the substrates were placed in a fume hood and dried for 12 h. We denote the modified substrates as mPANs.

Synthesis of polymers

The illustration of the synthesis of bromo-functionalized polyimide (PI-Br) are shown in Fig. S1.[35,36] Firstly, we synthesis the pristine 6FDA-DAM via step growth polymerization.[35] Before the reaction, purified 6FDA and DAM were dried under vacuum at 120 °C and 40 °C for 8 h. The monomer solution was prepared by adding 10 mmol 6FDA and 10 mmol DAM in a 100 mL bottle with 25.5 mL DMAc. The ratio of the monomers in the solution is 20 wt%. The solution was kept in 0°C, stirring by the mechanical stirrer at 800 rpm under Ar atmosphere for 24 h. Then the yellow colloidal solution was stirring at 25°C under Ar purge for another 24 h by adding acetic anhydride and triethylamine. After reaction, we precipitated and washed the dark yellow solution in methanol and placed the white polymer powder in a vacuum oven at 180 °C overnight to remove the absorbed water and solvent residues.

Secondly, we dissolved 6mmol self-made 6FDA-DAM powder in 50 ml CH_2Cl_2, stirring under N_2 purge. Then we added 6mmol NBS and 0.04 mmol AIBN to the mixture, and performed the reaction at 80°C for 4 h under reflux condensation. Following this, we precipitated and washed the product mixture in cold methanol and placed the light-yellow polymer powder under vacuum at 180 °C overnight to remove the absorbed water and solvent residues. The ^{1}HNMR results are shown in Fig. S2 and indicate the successful synthesis of PI-Br.

Synthesis of MOF nanocrystals

In this work, we synthesized amino-functionalized ZIF-8 nanocrystals (NH2-ZIF-8) via an improved mixed-linker strategy by modulating the reaction temperature.[15,37-39] First, we dissolved 34 mmol 2-methylimidazole, 6 mmol 2-aminobenzimidazole and 10 mmol sodium formate in 100 ml deionized water, under 70°C and stirred for 2 h. Second, we dissolved 10 mmol $Zn(NO_3)_2{\cdot}6H_2O$ in 100 ml DMF and stirring for 5 min. Then we mixed the above solutions and stirred for 1 h. After reaction, the MOF crystals were collected by centrifugation, washed several times in methanol and placed under vacuum at 85 °C overnight.

Preparation of MMCMs

We employed spin-coating method for the preparation of MMCMs.[40,41] In this study, we utilize nano-sized NH2-ZIF-8 crystals as MOF fillers, distributed in 6FDA-DAM or PI-Br, wherein the corresponding MMMs are denoted as MMCM-A and MMCM-B, respectively. To further reduce the thickness of the thin films, we increased the spin-coating speed and employed NH2-ZIF-8 with smaller size. Firstly, for MMCM-A, we placed the 6FDA-DAM powder under vacuum at 180 °C overnight. Moreover, we employed MOF/THF suspension rather than MOF powder to facilitate dispersing the MOF nanocrystals in the polymer solution. To prepare MMCMs with a certain filler composition, we dropped the MOF/THF suspension into a certain volume of 6FDA-DAM/THF solution (4 wt% of 6FDA-DAM) wherein MOF crystals accounts for 10-40 wt% to the total amount of MOF and 6FDA-DAM. Then we stirred the resulting solutions overnight and sonicated them for 3 h to eliminate the bubbles.

Secondly, we fixed the mPANs on the glass plates by Kapton tapes and placed the plates on the spin-coating machine. Then we spread the solution onto the whole area of mPANs and started spin-coating for 50 s at the speed of 1000 rpm. We employed NH2-ZIF-8 nanocrystals (mean diameter of ˜133 nm), with increasing the spinning speed to 2000 rpm to obtain MMCM-A with a thinner selective layer. Following this, we placed the membranes under vacuum at 40°C overnight.

Fabrication of MMCM-B was conducted by a similar protocol. The prepared NH2-ZIF-8/THF suspension was distributed into a dilute PI-Br/THF solution (4 wt% of PI-Br). In spin-coating process, we coated the solution onto the whole area of mPANs and started spin-coating for 50 s at the speed of 2000 rpm. Similar with MMCM-A, we employed NH2-ZIF-8 with mean size of ˜82 nm and increased the spinning speed to 3000 rpm to obtain MMCM-B with thinner selective layers. After the spin-coating process, we placed the membranes under vacuum at 40°C overnight.

Characterization

The surface area and pore structure of the synthesized NH2-ZIF-8 samples was measured by Micromeritics instrument (ASAP 2460) under N_2 sorption at 77 K. The morphologies of the NH2-ZIF-8 nanocrystals and the membranes were characterized by Scanning electron microscopy (SEM) (Regulus R-8100). The X-ray diffraction (XRD) spectrum of NH2-ZIF-8 were characterized on Rigaku D/max 2500v/pc using Cu Kα radiation. Before analyzing the surface area, we degassed NH2-ZIF-8 nanocrystals at 120°C overnight. The interfacial interactions in MMCMs were characterized by Fourier Transform Infrared (FT-IR, Bruker Vertex 70). The cross-sections of the MMCMs were prepared under freezing conditions wherein the membranes were fractured after being immersed in liquid N_2 for 120 s. Before characterization, we coated the SEM samples with Platinum to increase the conductivity.

Results and Discussion

Characterization of NH2-ZIF-8 nanocrystals

In this study, we synthesized three types of NH2-ZIF-8 nanocrystals with different sizes.[37-39] As shown in Fig.2a, the XRD patterns of synthesized NH2-ZIF-8 nanoparticles are all consistent with the simulated pattern, confirming the successful synthesis. The SEM images of NH2-ZIF-8 nanocrystals show that the three types of synthesized NH2-ZIF-8 crystals have size of 82±18 nm (Fig. 2b), 133±15 nm (Fig. 2c) and 245±70 nm (Fig. 2d), respectively. We employed N_2 adsorption measurement to examine the pore structures of the NH2-ZIF-8 samples. According to the results in Fig. 2e, we calculate the BET surface areas of the NH2-ZIF-8 nanocrystals are 985.4 cm^2 g^{-1}, 625.2 cm^2g^{-1} and 460.7 cm^2g^{-1}, respectively, indicating a high gas adsorption capacity which facilitates the low-resistance molecular diffusion. As shown in Fig. 2f, it can be found that new infrared absorption peaks exist at 3183 and 3381cm^{-1}, corresponding to the stretching vibration of -N-H, confirming the successful incorporation of amino groups in ZIF-8 crystals.

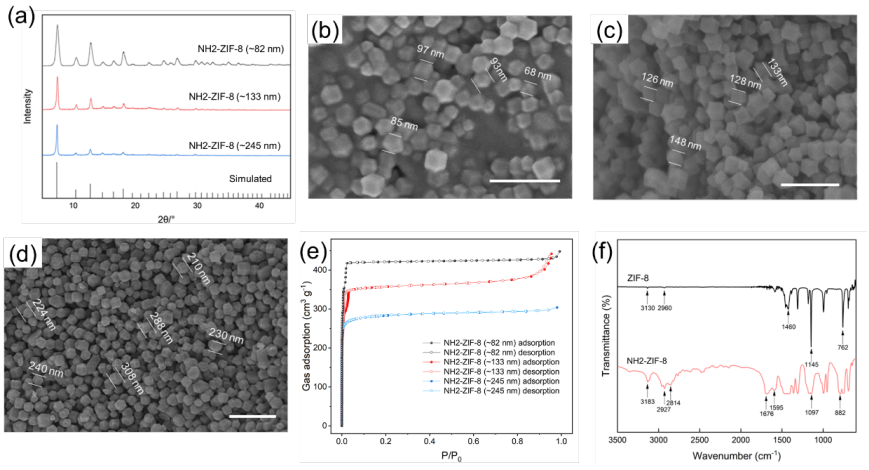

Fig.2 Characterization of the synthesized NH2-ZIF-8 samples. (a) XRD patterns. (b-d) SEM images of NH2-ZIF-8 crystals with mean size of (b) 82 nm, (c) 133 nm and (d) 245 nm, scale bar=500 nm, (e) N_2 adsorption isotherms at 77 K, (f) FTIR spectrum of ZIF-8 and NH2-ZIF-8.

Fabrication and characterization of MMCMs

Highly permeable porous substrates are critical to fabricating MMCMs, and the gutter layer on the substrates has been regarded to provide a smooth surface and avoid the penetration of the dilute solution into the pores of substrates.[4,42] In this work, we employed crosslinked polydimethylsiloxane (PDMS) as the gutter layer and precoated it onto the PAN substrates via spin-coating. As shown in Fig. S3, we successfully fabricated modified substrates with a gutter layer of ˜100 nm thick and the CO_2 permeance is ˜10000 GPU, wherein the trans-membrane resistance is negligible.

We fabricated the MMCMs through spin-coating, and the thickness of top selective layer could be controlled by adjusting the spinning speed. Herein, we employed NH2-ZIF-8 nanoparticles as MOF fillers, distributed in 6FDA-DAM or bromo-functionalized polyimide (PI-Br), wherein the MMMs are denoted as MMCM-A and MMCM-B, respectively. To further reduce the thickness of the top layer, we increase the spin-coating speed and employed NH2-ZIF-8 with smaller size.

We employed SEM to observe the cross-sectional and surface morphologies of MMCMs. As shown in Fig.3a-c, the MOF-protruding structure was formed in MMCM-A. The cross-sectional images show that the selective layer is ˜280 nm thick (Fig. 3a-b), and MOF crystals could protrude the polyimide matrix. The surface SEM image (Fig. 3c) shows the clear rhombic facets of NH2-ZIF-8 crystals appearing on the thin film and no defects or pinholes were generated during the membrane fabrication. The cross-sectional images of the MMCM-A with a thinner selective layer is shown in Fig 3d-e. With a MOF loading of 20 wt%, the selective layer of MMCM-A is ˜150 nm thick, while NH_2-ZIF-8 crystals could also nearly penetrate the whole thickness. However, it is noteworthy that lots of pinholes appearing on the surface of the film, resulting in non-selective defects which could cause a significant decrease in gas selectivity (Fig. 3f).

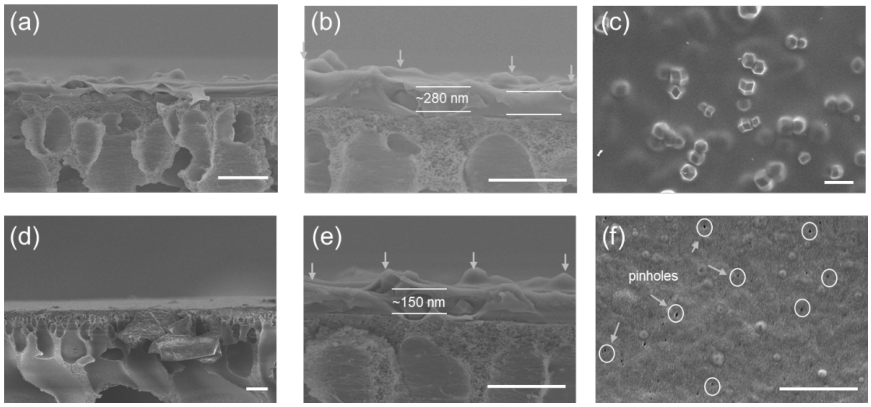

Fig. 3 Characterization of MMCM-A (20 wt% MOF loading). Morphologies of MMCM-A at spinning speed of 1000 rpm: (a, b) cross-sectional images, (c) surface image. Morphologies of MMCM-A at spinning speed of 2000 rpm: (d, e) cross-sectional images, (f) surface image. (Scale bar=500 nm)

With regard to MMCM-B, the MOF-protruding structure could also be observed. The cross-sectional images (Fig. 4a-b) show that the selective layer is only ˜140 nm thick, and NH2-ZIF-8 crystals could nearly penetrate the polymer matrix. Moreover, we notice that facets of NH2-ZIF-8 crystals appearing on the thin film and no defects or pinholes were generated (Fig.4c). The cross-sectional images of the MMCM-B with a thinner selective layer is shown in Fig 4d-e. The selective layer is ˜80 nm thick, and NH2-ZIF-8 crystals could nearly penetrate the selective layer, while defects and pinholes appear on the membrane surface (Fig. 4f), which are detrimental to the separation performance.

The FT-IR spectra clearly demonstrate the interfacial interactions in MMCMs. As shown in Fig. S4, aromatic imide structure exists in polyimide at 1780 and 1720 cm^{-1}, indicating the asymmetric and symmetric stretching vibration of C=O, respectively. The peak corresponding to the stretching vibration of C-N in

imide rings appears at 1357 cm^{-1}, and the peak corresponding to the bending vibration of C=O appears at 720 cm^{-1}. Compared with pure 6FDA-DAM, the imide characteristic peak of the MMCM-A remains after the incorporation of NH2-ZIF-8 crystals, confirming the existence of the chemical structure of polyimide. Moreover, the C=O characteristic peak of the MMCM-A exhibits a slight blue shift, confirming the hydrogen-bonding interaction between the amine groups of MOF particles and polyimide chains.

Fig. S5 shows the infrared spectra of PI-Br and MMCM-B with different MOF loading. The characteristic peak of imide ring retains in the membranes, indicating the existence of polyimide structure. Meanwhile, the peak corresponding to the stretching vibration of C-Br appears at 650 cm^{-1}, confirming the successful functionalization of bromine on 6FDA-DAM chains. In contrast with the infrared absorption peak of MOF crystals, the peaks of the amine weaken after crosslinking, while the band strength of the aryl-N increases, confirming the covalent-bonding exist between PI-Br and NH2-ZIF-8.

Overall, through optimizing the fabrication parameters, we prepared pinhole-free MMCM-A and MMCM-B wherein the membrane thickness is ˜280 and ˜140 nm, respectively. Because the interfacial covalent bonds in MMCM-B are much stronger than the hydrogen bonds in MMCM-A, wherein the stronger interfacial bonds benefit the formation of compatible interface structure, MMCM-B membrane materials could be manufactured into much thinner film.

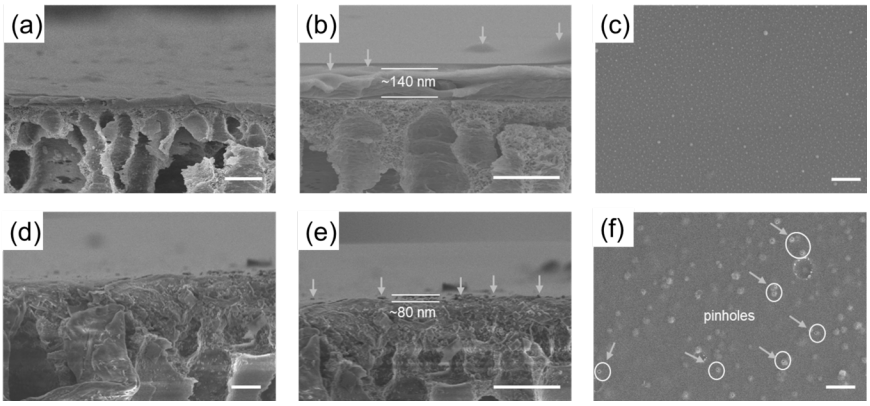

Fig. 4 Characterization of MMCM-B (20 wt% MOF loading). Morphologies of MMCM-B at spinning speed of 2000 rpm: (a, b) cross-sectional images, (c) surface image. Morphologies of MMCM-B at spinning speed of 3000 rpm: (d, e) cross-sectional images, (f) surface image. (Scale bar=500 nm)

2.4 Gas separation performance

The transport properties of 30/70 (v/v) CO_2/CH_4 mixture of the MMCMs were evaluated. The separation performance of MMCMs has a strong dependence on the MOF loading as clearly shown in Fig. 5a and b. The CO_2 permeance of 6FDA-DAM membranes with a 300-nm thickness is 242 GPU, with a CO_2/CH_4selectivity of 26. When the MOF loading increases to 20 wt%, the CO_2 permeance of MMCM-A increases to 642 GPU, with the CO_2/CH_4 selectivity slightly increasing to 33 (Fig. 5a). Fig. 5b shows the separation performance of MMCM-B with different NH2-ZIF-8 loading (0 to 40 wt%). With increasing the NH2-ZIF-8 loading from 0-20 wt%, the MMCM-B exhibits a drastically enhanced CO_2 permeance (from 304 to 778 GPU) and an increased CO_2/CH_4 selectivity (from 22 to 34). This is possibly due to the protruding amino-functionalized MOF crystals with high specific surface area fortified the CO_2 adsorption and solution processes and facilitate the low-resistance diffusion of gas molecules. Moreover, the selectivity of all the MMCMs declines drastically with the NH2-ZIF-8 loading increasing to over 30 wt%, owing to the crystal aggregation and the generation of interfacial voids, wherein non-selective diffusion reduces the selectivity.

Plasticization effect of polymer-based membranes is also a challenging problem in industrial applications.[24,33,34,43,44] In general, under high pressure, polar gas molecules with high critical temperatures

such as CO_2, C_2H_4 and C_3H_6 can swell and promote the mobility of the polymer chains, resulting in a significant drop of the selectivity and a slight increase of the permeance. To evaluate the plasticization-resistant properties, we utilized the plasticization point which refers to the pressure wherein the CO_2permeance upturns.[44] In this regard, we tested the separation performance of MMCMs under equimolar mixed gas with CO_2 partial pressure increasing to 20 bar. For 6FDA-DAM membrane, the plasticization point appears at CO_2partial pressure of 15 bar, wherein the CO_2 permeance reaches its minimum value of 66 GPU (Fig. 5c). With regard to the MMCMs, both the CO_2 permeance of MMCM-A and MMCM-B decreases monotonically and we did not observe a plasticization point. It is noteworthy that when the CO_2 partial pressure increasing to 20 bar, the CO_2/CH_4 selectivity of polyimide, MMCM-A and MMCM-B decreases by 71.2%, 54.9% and 28.5% (Fig. 5d), respectively. Overall, the above results show that MMCMs yield a significant plasticization resistant performance. Moreover, because the interfacial covalent bonds in MMCM-B are much more robust than the hydrogen bonds in MMCM-A membranes, wherein the stronger interfacial bonds potentially restrict the swelling of polyimide chains at high feed gas pressure, MMCM-B exhibits a superior pressure stability.

Aging effect in polymeric membranes is another challenging problem for practical applications,[29,43,44] which is typically prominent in thin-film glassy polymers.[18,33,45-47] We tested the long-term stabilities of the MMCMs for nearly one month. As shown in Fig. 5e-f, the pure polyimide membranes exhibit a typical aging performance, and the CO_2 permeance decreases 64.5% after 28 days, from 242 to 86 GPU. In contrast, the MMCMs exhibited an improved aging-resistance performance. For MMCM-A, the CO_2 permeance reduces from 652 to 417 GPU, with 36% of declination after 28 days. With regard to MMCM-B, the CO_2 permeance decreases from 778 to 583 GPU, retaining 75% of the initial separation performance. The above results indicate that the MMCM-B with robust covalent-bonding exhibit a better long-term stability for nearly one month than the MMCM-A with hydrogen-bonding and pure polyimide membranes.

As shown in Fig. 6, compared with the state-of-the-art composite membranes, the MMCMs exhibit an outstanding CO_2/CH_4 separation performance. The yellow dashed lines in Fig 6 depict the target performance zone of CO_2/CH_4 separation membranes, indicating that a membrane should yield a CO_2 permeance higher than 100 GPU and a CO_2/CH_4selectivity higher than 30 to achieve economical demands for natural gas purification.[48] The separation performances of both MMCM-A and MMCM-B surpass all the polyimide-based composite membranes and the MMCMs reported in the literature and are comparable to the facilitated transport membranes.

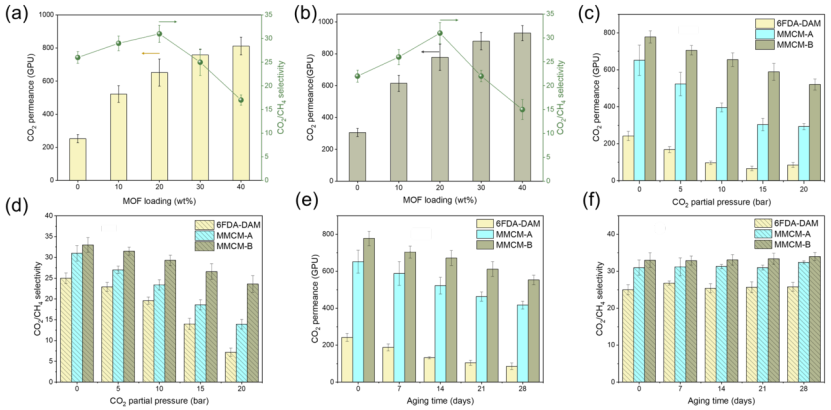

Fig. 5 Gas separation performance of MMCMs. Effect of MOF loading on CO_2 permeance and CO_2/CH_4 selectivity (feed gas: CO_2/CH_4 = 3/7 vol% mixed gas, 1 bar) of (a) MMCM-A, (b)MMCM-B. Effect of CO_2 partial pressure on separation performance of pristine polyimide, MMCM-A and MMCM-B (equimolar mixed gas, 30°C): (c) CO_2 permeance, (d) CO_2/CH_4 selectivity. Long-term stability of pristine polyimide, MMCM-A and MMCM-B (feed gas: CO_2/CH_4 = 3/7 vol% mixed gas, 1 bar, 30°C): (e) CO_2 permeance, (f)

CO_2/CH_4 selectivity.

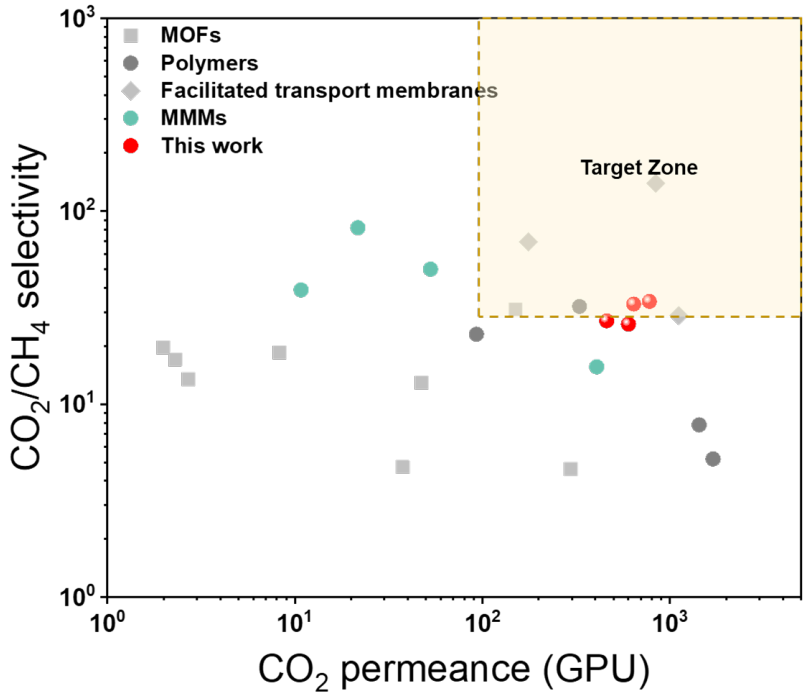

Fig. 6 Comparison of the CO_2/CH_4 separation performance of the MMCMs with the state-of-the-art composite membranes (Table S1). The yellow dashed line shows the target zone for membrane-based purification of natural gas (CO_2 permeance > 100 GPU, CO_2/CH_4 selectivity > 30)[48].

4. Conclusion

In conclusion, an ultrathin mixed matrix composite membrane (MMCM) with NH2-ZIF-8 nanocrystals protruding structure was successfully fabricated. Through engineering the polyimide/MOF interfacial hydrogen or covalent bonds, the thickness of the selective layer can be reduced to 280 or 140 nm. The protruding MOF filler can considerably reduce the transport resistance and promote the CO_2 permeation. As a result, the MMCMs exhibit a high CO_2 permeance of 778 GPU and a CO_2/CH_4 selectivity of 34, surpassing most of the reported MOF-based MMMs and polyimide composite membranes towards CO_2/CH_4 separation. Moreover, due to the robustness of the interfacial interactions between MOFs and the polymer chains in the thin films, the MMCMs show a significantly enhanced plasticization-resistant and aging-resistant performance at a high CO_2 partial pressure up to 20 bar and exhibit a long-term stability for nearly one month. Overall, this work demonstrates an efficient and general strategy to fabricate advanced ultrathin mixed matrix composite membranes with both high separation performance and excellent stabilities under high pressure, which hold great potential to address many critical separation issues in chemical industry.

Acknowledgements

We sincerely appreciate the generous support of the National Natural Science Foundation of China (21838008, U20B2023, 21621004, 21878215, 21490583), National Key R & D Program of China (2017YFB 0603400), Program of Introducing Talents of Discipline to Universities (No. BP0618007), State Key Laboratory of Materials-Oriented Chemical Engineering (ZK202002) and the Haihe Laboratory of Sustainable Chemical Transformations.

References

1. Sholl DS, Lively RP. Seven chemical separations to change the world.*Nature* . 2016; 532(7600): 435. doi: 10.1038/532435a

2. Sandru M, Sandru EM, Ingram WF, et al. An integrated materials approach to ultrapermeable and ultraselective CO2 polymer membranes.*Science* . 2022; 376(6588): 90-94. doi: 10.1126/science.abj9351

3. Wang H, Wang M, Liang X, et al. Organic molecular sieve membranes for chemical separations. *Chem Soc Rev* . 2021; 50(9): 5468-5516. doi: 10.1039/d0cs01347a

4. Qiao Z, Zhao S, Sheng M, et al. Metal-induced ordered microporous polymers for fabricating large-area gas separation membranes. *Nat Mater* . 2019; 18(2): 163-168. doi: 10.1038/s41563-018-0221-3

5. Liu Y, Wu H, Wu S, et al. Multifunctional covalent organic framework (COF)-Based mixed matrix membranes for enhanced CO2 separation. *J Membr Sci* . 2021; 618: 118693. doi: 10.1016/j.memsci.2020.118693

6. Guo Z, Wu H, Chen Y, et al. Missing-linker defects in covalent organic framework membranes for efficient CO2 separation. *Angew Chem Int Ed* . 2022: e202210466. doi: 10.1002/anie.202210466

7. Guo Z, Jiang H, Wu H, et al. Oil-water-oil triphase synthesis of ionic covalent organic framework nanosheets. *Angew Chem Int Ed* . 2021; 60(52): 27078-27085. doi: 10.1002/anie.202112271

8. Yang L, Yang H, Wu H, et al. COF membranes with uniform and exchangeable facilitated transport carriers for efficient carbon capture. *J Mater Chem A* . 2021; 9(21): 12636-12643. doi: 10.1039/d0ta12486a

9. Park HB, Jung CH, Lee YM, et al. Polymers with cavities tuned for fast selective transport of small molecules and ions. *Science* . 2007; 318(5848): 254-258. doi: 10.1126/science.1146744

10. Lai HWH, Benedetti FM, Ahn JM, et al. Hydrocarbon ladder polymers with ultrahigh permselectivity for membrane gas separations.*Science* . 2022; 375(6587): 1390-1392. doi: 10.1126/science.abl7163

11. Guiver MD, Lee YM. Polymer rigidity improves microporous membranes.*Science* . 2013; 339(6117): 284-285. doi: 10.1126/science.1232714

12. Robeson LM. The upper bound revisited. *J Membr Sci* . 2008; 320(1-2): 390-400. doi: 10.1016/j.memsci.2008.04.030

13. Robeson LM. Correlation of separation factor versus permeability for polymeric membranes. *J Membr Sci* . 1991; 62(2): 165-185. doi: 10.1016/0376-7388(91)80060-J

14. Wang Y, Wang X, Guan J, et al. 110th anniversary: mixed matrix membranes with fillers of intrinsic nanopores for gas separation.*Ind Eng Chem Res* . 2019; 58(19): 7706-7724. doi: 10.1021/acs.iecr.9b01568

15. Park S, Jeong H-K. In-situ linker doping as an effective means to tune zeolitic-imidazolate framework-8 (ZIF-8) fillers in mixed-matrix membranes for propylene/propane separation. *J Membr Sci* . 2020; 596: 117689. doi: 10.1016/j.memsci.2019.117689

16. Diestel L, Wang NY, Schwiedland B, Steinbach F, Giese U, Caro J. MOF based MMMs with enhanced selectivity due to hindered linker distortion.*J Membr Sci* . 2015; 492: 181-186. doi: 10.1016/j.memsci.2015.04.069

17. Caro J. Are MOF membranes better in gas separation than those made of zeolites? *Curr Opin Chem Eng* . 2011; 1(1): 77-83. doi: 10.1016/j.coche.2011.08.007

18. Bae TH, Lee JS, Qiu WL, Koros WJ, Jones CW, Nair S. A high-performance gas-separation membrane containing submicrometer-sized metal-organic framework crystals. *Angew Chem Int Ed* . 2010; 49(51): 9863-9866. doi: 10.1002/anie.201006141

19. An H, Cho KY, Lyu Q, et al. Facile defect engineering of zeolitic imidazolate frameworks towards enhanced C3H6/C3H8 separation performance. *Adv Funct Mater* . 2021; 31: 2105577. 2105577. doi: 10.1002/adfm.202105577

20. Liu Y, Wu H, Li R, et al. MOF-COF "alloy" membranes for efficient propylene/propane separation. *Adv Mater* . 2022: e2201423. doi: 10.1002/adma.202201423

21. Wu X, Ren Y, Sui G, et al. Accelerating CO2 capture of highly permeable polymer through incorporating highly selective hollow zeolite imidazolate framework. *AIChE J* . 2020; 66(2): e16800. doi: 10.1002/aic.16800

22. Ma X, Wu X, Caro J, Huang A. Polymer composite membrane with penetrating ZIF-7 sheets displays high hydrogen permselectivity.*Angew Chem Int Ed* . 2019; 58(45): 16156-16160. doi: 10.1002/anie.201911226

23. Wang B, Qiao Z, Xu J, et al. Unobstructed ultrathin gas transport channels in composite membranes by interfacial self-assembly. *Adv Mater* . 2020; 32(22): e1907701. doi: 10.1002/adma.201907701

24. Song S, Jiang H, Wu H, et al. Weakly pressure-dependent molecular sieving of propylene/propane mixtures through mixed matrix membrane with ZIF-8 direct-through channels. *J Membr Sci* . 2022; 648: 120366. doi: 10.1016/j.memsci.2022.120366

25. Shu L, Peng Y, Yao R, Song H, Zhu C, Yang W. Flexible soft-solid metal-organic framework composite membranes for H2 /CO2 separation.*Angew Chem Int Ed* . 2022: e202117577. doi: 10.1002/anie.202117577

26. Xie K, Fu Q, Xu C, et al. Continuous assembly of a polymer on a metal–organic framework (CAP on MOF): a 30 nm thick polymeric gas separation membrane. *Energy Environ Sci* . 2018; 11(3): 544-550. doi: 10.1039/c7ee02820b

27. Fu Q, Kim J, Gurr PA, Scofield JMP, Kentish SE, Qiao GG. A novel cross-linked nano-coating for carbon dioxide capture. *Energy Environ Sci* . 2016; 9(2): 434-440. doi: 10.1039/c5ee02433a

28. Xie K, Fu Q, Webley PA, Qiao GG. MOF scaffold for a high-performance mixed-matrix membrane. *Angew Chem Int Ed* . 2018; 57(28): 8597-8602. doi: 10.1002/anie.201804162

29. Rowe BW, Freeman BD, Paul DR. Physical aging of ultrathin glassy polymer films tracked by gas permeability. *Polymer* . 2009; 50(23): 5565-5575. doi: 10.1016/j.polymer.2009.09.037

30. Du N, Park HB, Robertson GP, et al. Polymer nanosieve membranes for CO2-capture applications. *Nat Mater* . 2011; 10(5): 372-375. doi: 10.1038/NMAT2989

31. Yong WF, Li FY, Xiao YC, Chung TS, Tong YW. High performance PIM-1/Matrimid hollow fiber membranes for CO2/CH4, O2/N2 and CO2/N2 separation. *J Membr Sci* . 2013; 443: 156-169. doi: 10.1016/j.memsci.2013.04.037

32. Koros WJ, Fleming GK. Membrane-based gas separation. *J Membr Sci* . 1993; 83(1): 1-80. doi: 10.1016/0376-7388(93)80013-N

33. Cheng Y, Wang X, Jia C, et al. Ultrathin mixed matrix membranes containing two-dimensional metal-organic framework nanosheets for efficient CO2/CH4 separation. *J Membr Sci* . 2017; 539: 213-223. doi: 10.1016/j.memsci.2017.06.011

34. Bachman JE, Smith ZP, Li T, Xu T, Long JR. Enhanced ethylene separation and plasticization resistance in polymer membranes incorporating metal-organic framework nanocrystals. *Nat Mater* . 2016; 15(8): 845-9. doi: 10.1038/nmat4621

35. Wang L, Cao Y, Zhou M, Zhou SJ, Yuan Q. Novel copolyimide membranes for gas separation. *J Membr Sci* . 2007; 305(1-2): 338-346. doi: 10.1016/j.memsci.2007.08.024

36. An H, Lee AS, Kammakakam I, et al. Bromination/debromination-induced thermal crosslinking of 6FDA-Durene for aggressive gas separations.*J Membr Sci* . 2018; 545: 358-366. doi: 10.1016/j.memsci.2017.09.083

37. Schejn A, Balan L, Falk V, Aranda L, Medjahdi G, Schneider R. Controlling ZIF-8 nano- and microcrystal formation and reactivity through zinc salt variations. 10.1039/C3CE42485E. *CrystEngComm* . 2014; 16(21): 4493-4500. doi: 10.1039/C3CE42485E

38. Yeung HH-M, Sapnik AF, Massingberd-Mundy F, et al. Control of metal-organic framework crystallization by metastable intermediate pre-equilibrium Species. *Angew Chem Int Ed* . 2019; 58(2): 566-571. doi: 10.1002/anie.201810039

39. Wang J, Wang Y, Liu Y, et al. Ultrathin ZIF-8 membrane through inhibited ostwald ripening for high-flux C3H6/C3H8 separation. *Adv Funct Mater* . 2022: 2208064. doi: 10.1002/adfm.202208064

40. Liu Y, Wu H, Min L, et al. 2D layered double hydroxide membranes with intrinsic breathing effect toward CO2 for efficient carbon capture.*J Membr Sci* . 2020; 598: 117663. 117663. doi: 10.1016/j.memsci.2019.117663

41. Li B, You X, Wu H, et al. A facile metal ion pre-anchored strategy for fabrication of defect-free MOF membranes on polymeric substrates.*J Membr Sci* . 2022; 650120419. doi: 10.1016/j.memsci.2022.120419

42. Dong S, Wang Z, Sheng M, Qiao Z, Wang J. Scaling up of defect-free flat membrane with ultra-high gas permeance used for intermediate layer of multi-layer composite membrane and oxygen enrichment. *Sep Purif Technol* . 2020; 239 doi: 10.1016/j.seppur.2020.116580

43. Yong WF, Kwek KHA, Liao KS, Chung TS. Suppression of aging and plasticization in highly permeable polymers. *Polymer* . 2015; 77: 377-386. doi: 10.1016/j.polymer.2015.09.075

44. Wu Y, Guo Z, Wu H, et al. Plasticization- and aging-resistant membranes with venation-like architecture for efficient carbon capture.*J Membr Sci* . 2020; 609 doi: 10.1016/j.memsci.2020.118215

45. Liu G, Chernikova V, Liu Y, et al. Mixed matrix formulations with MOF molecular sieving for key energy-intensive separations. *Nat Mater* . 2018; 17(3): 283-289. doi: 10.1038/s41563-017-0013-1

46. Liu Z, Liu Y, Liu G, Qiu W, Koros WJ. Cross-linkable semi-rigid 6FDA-based polyimide hollow fiber membranes for sour natural gas purification. *Ind Eng Chem Res* . 2020; 59(12): 5333-5339. doi: 10.1021/acs.iecr.9b04821

47. Jiang H, Chen Y, Song S, et al. Confined facilitated transport within covalent organic frameworks for propylene/propane membrane separation. *Chem Eng J* . 2022; 439: 135657. doi: 10.1016/j.cej.2022.135657

48. Merkel TC, Lin H, Wei X, Baker R. Power plant post-combustion carbon dioxide capture: An opportunity for membranes. *J Membr Sci* . 2010; 359(1-2): 126-139. doi: 10.1016/j.memsci.2009.10.041